**Solid Freeform Fabrication 2022: Proceedings of the 33rd Annual International Solid Freeform Fabrication Symposium – An Additive Manufacturing Conference**
**Reviewed Paper**

# INDUCTION INITIATED CURING OF ADDITIVELY MANUFACTURED THERMOSET COMPOSITES

L. Omer*, M. J. Uddin*, H. Chowdhury*, J. Martinez*, I. Sporn*, B. Dudek* and J. Tate*†

*Ingram School of Engineering
† Materials Science Engineering and Commercialization Program
†Email: JT31@txstate.edu Phone: (512) 245-1826

## ABSTRACT

Additive Manufacturing (AM) has provided a new potential for material customization through the reduction in geometric constraints of products. The freeform geometry produced using AM allows for the creation of optimized structural parts that reduce weight and material waste. In addition, AM reduces production time by providing a model to product workflow with limited requirements for tooling and machine setup in advance. However, current work in printing thermoset composite parts is limited. One of the confounding factors in the AM of thermoset composites involves in situ curing of the composite resin system. This research proposes the creation of an additive manufacturing process for thermoset composites based upon induction initiated thermoset curing. The use of induction-based curing will allow the production of parts without the normal constraint of either oven or autoclave curing. A rapid curing resin system will be reinforced using milled fiber reinforcement and doped with a ferromagnetic susceptor to induce homogenous heating and curing of the resin in situ. The resulting composite will be evaluated for mechanical performance versus oven cure samples. Scanning electron microscopy in tandem with energy dispersive x-ray spectroscopy will be used to validate homogenous particle dispersion. Lastly, differential scanning calorimetry will be used to compare the degree of polymer conversion between induction and conventional curing.

Keywords: Fused Filament Fabrication, Thermoset Curing, Advanced Composites, Additive Manufacturing, Polymer Matrix Composites, Induction Heating

## 1. INTRODUCTION

The design and fabrication of lightweight composite materials are gaining popularity because of their enormous potential to replace traditional structural materials. The fact that weight reduction may be increased with topology optimization without sacrificing structural performance has sparked renewed interest in additive manufacturing (AM). Material production with complicated geometries is possible with this method. As a result of this versatile style of manufacturing, components can be altered, and their weights can be reduced without compromising the component's functionality. Continuous fiber-reinforced polymer composites headline the potential in this area since their mechanical properties are comparable to the metals, having significantly lower density [1].

However, there are physical and processing limits in additive manufacturing of polymer composites reinforced with continuous fibers, including a minimum deposition length and minimal corner radius [2]. Manufacturing with short fibers provides much more flexibility in fiber

positioning and material deposition, resulting in easier material processing. The lower material costs and void content of short fiber composites, make them an appealing solution for many AM applications.

The fused filament fabrication (FFF) additive manufacturing technology was utilized to develop short fiber-reinforced composites by melting and extruding a thermoplastic polymer matrix. According to Nawafleh's Additive manufacturing of short fiber reinforced thermoset composites [1], the addition of short fibers to a plain, unreinforced thermoplastic matrix resulted in a considerable improvement in tensile strength and elastic modulus in several of these research studies. Although thermoplastic composites with significant quantities (40%) of short fibers could be produced and 3D-printed well enough, the maximum tensile strength of these composites was still limited (100 MPa). This was attributed to poor interfacial adhesion between the fibers and the thermoplastic matrix, as well as porosity between the print lines (which was unavoidable in the FFF process). As demonstrated in Figure 1, these processing difficulties limited the strength and hence the applications of additively manufactured thermoplastic composites.

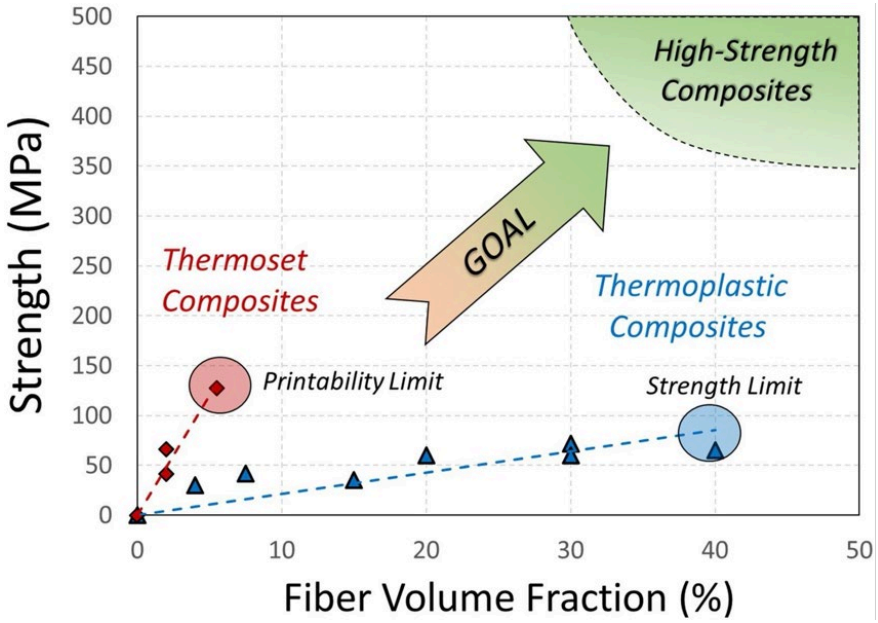


Figure 1. Strength versus fiber volume fraction chart on the short fiber reinforced thermoplastic and thermoset composites. From Nawafleh's AM study [1].

The liquid resin in thermoset composites can moisten the fiber surface, facilitating the chemical bonding process. The direct write technique is used for liquid thermoset materials additive manufacturing of process instead of the FFF process, which is dependent on polymer melting and solidification. Viscous pastes are formed by combining liquid polymer resins with fiber reinforcements and rheology-modifying nanoparticles and then extruding them into the desired geometries. Finally, the extruded material is cured into solid structures by heat or light. In 2014, Compton and Lewis presented direct write additive manufacturing to construct carbon-fiber reinforced epoxy composites, and it has since been used by other research groups to fabricate various thermoset reinforced composites with short carbon or Kevlar fibers [3]. When the same

amount of fiber loading is used, it is obvious from Fig. 1 that additively manufactured thermoset composites are stronger than thermoplastic composites.

Additive manufactured short carbon-fiber reinforced composites have the potential to replace common structural metals like aluminum and low-strength steels, resulting in significant weight reduction. The mechanical characteristics of these materials may be improved even more by fine-tuning the additive manufacturing settings and minimizing flaws caused by a large number of pores in the current specimens. Compression testing showed that removing these flaws will improve the mechanical performance of these composite structures substantially.

In summary, due to the high amount of porosity and inadequate adhesion between the thermoplastic polymer and the fibers in these materials, short fiber reinforced thermoplastic composites are strength-limited, as illustrated in Figure 1. Because of the good chemical interaction between the fibers and the thermoset matrix, as well as their low porosity, thermoset composites have substantially greater strength. However, additive fabrication of these systems is exceedingly challenging at 5% fiber loading, which is necessary to obtain significant levels of mechanical strength and stiffness.

Typical processing of polymer matrix composite materials involves curing using heat transfer to get a complete cure. This is often done in convection ovens, by heating the surrounding air of a composite. It can also lead to agglomeration of nanoparticles that may be added for the purpose of increasing various properties of the composite, such as increased mechanical strength. The Army concluded that a process called induction heating may be a solution to this issue, as the manipulation of ferrimagnetic particles may be able to cure a composite in a more uniform manner, making the product more isotropic [4]. These magnetic materials, called susceptors, heat up when exposed to these electromagnetic fields. During this magnetization-demagnetization cyclic process, hysteresis losses occur if the material is magnetic, causing heating [4].

Induction heating of ferrimagnetic nanoparticles in a self-healing thermoplastic adhesive is used to enable magnetic induction heating, while also enhancing the lap-shear strength of the adhesive. By utilizing the hysteresis loss mechanism, strong bonds between carbon fiber composites are achieved by repeatedly bonding and debonding the adhesive. One experiment achieved a bonding strength that was higher than any other thermoplastic based adhesives reported to date [5].

The use of induction heating may be a solution to the curing issue, but due to the complex ratio of particles the mechanical properties of the samples were shown to have mixed changes in performance in Thomas Bayerl's study on induction heating of thermoplastics [6]. When compared to neat samples, the tensile properties would decrease, while the Young's modulus would increase across all filler ratios. The other property change was an increase in brittleness of the material leading to a 25% decrease in notched impact strength [6].

Although electromagnetic induction offers high energy density and the ability to heat selectively and uniformly, this cannot be obtained without the use of susceptor fillers to convert electromagnetic energy into heat. Proper ratios of reinforcement filler to susceptor filler to matrix material with adequate working temperature must be further explored for optimum mechanical properties of the material [7].

The motivation of our research is to determine a precise ratio of reinforcement fillers to magnetic susceptor to optimize curing time and maximize mechanical properties. We are primarily concerned with testing different loading levels of composites fillers using susceptor curing. Utilizing additive manufacturing, hysteresis loss mechanisms for curing are required to reduce the necessity of expensive and large oven curing system.

When a high temperature material is required that incorporates additive manufacturing and induction heating, we need multiple reinforcement fillers to satisfy various needs. These reinforcement fillers will be evenly dispersed to facilitate released exothermic heat and help cure the surrounding thermoset material as it is being printed. In terms of the filler material, $Fe_3O_4$ is used as a susceptor to allow for induction curing, due to its ferrimagnetic properties. Milled carbon fiber material is added to the material to provide an overall increase in mechanical properties, and graphitized micro balloons are added to increase the strength-to-weight ratio.

## 2. MATERIAL SYSTEMS

To produce our thermoset composites, we dried reinforcement fillers at 70°C in oven for 2 hours to reduce residual moisture and maintain resin temperature during mixing. We UHTR-9863S resin as our base matrix which was placed in a 70°C water bath for 30 minutes to ensure a workable resin viscosity. Once heated, Titanium Butoxide catalyst was added at 5 wt.% and evenly dispersed using hand mixing for two minutes followed by two minutes of high-speed mechanical mixing. Following catalyst dispersion, the preheated fillers were steadily mixed into the catalyzed resin and then mechanically mixed at 650 rpm for two minutes. After mixing, the mixed composite pastes were printed using Lutum V4 to produce samples of each material composition with dimensions of 12.5mm x 130mm x 6mm. The coupons were removed from the printer and set in the induction coil to cure the sample using induction curing. The coupons were also set in a convection oven at 250C for 2.5 hours to produce oven cured sample. The samples were then tested for porosity, tensile testing, particle aggregation.

For this project eight treatment groups were initially present, these groups were compared by the ratios of their filler materials in high or low concentrations as seen in Table 1. The filler material consisted of $Fe_3O_4$, Milled Carbon Fiber (MCF), and Graphitized micro balloons (GMB). Due to poor heat performance the low concentrations of $Fe_3O_4$ (--+, -+-, -++, and ---), the samples were not tested for their mechanical properties or morphology.


Figure 2. Treatment group samples (+--, +-+, +++, and ++-)

The four samples that were kept for experimentation were named in respect to the concentration value of the filler used. If a high concentration was used, it was denoted as + and if

low concentration was used it was denoted as -, and each followed the convention of $Fe_3O_4$ then MCF then GMB. The treatment groups were as follows: +--, ++-, +-+, and +++, and the concentration levels of each treatment group can be seen in detail in Table 1 below.

Table 1. Concentration levels of Filler Material in parts per hundred of UHTM resin

| Treatment Group | $Fe_3O_4$ Concentration | MCF Concentration | GMB Concentration |
|---|---|---|---|
| +-- | 30pph (High) | 20pph (Low) | 15pph (Low) |
| ++- | 30pph (High) | 30pph (High) | 15pph (Low) |
| +-+ | 30pph (High) | 20pph (Low) | 25pph (High) |
| +++ | 30pph (High) | 30pph (High) | 25pph (High) |

Following optimization of composite reinforcements, the effects of curing strategy on particle agglomeration was studied in the material composite yielding the highest performance. Identical composites of the (+++) composite were cured using either the previously mentioned oven curing or induction curing. Induction cure was performed using a 10 turn, 4-inch diameter solenoid coil mounted on a MTI corporation SP-25A heater for 9 minutes with a 50 KHz frequency and 0.165 Tesla magnetic field strength. Following curing, the materials were examined for particle degradation and dispersion within the resulting composites.

## 3. EXPERIMENTATION

### 3.1 TGA and DTGA

For each treatment group the thermal analysis was performed on the SDT650, which would perform both the DTGA and TGA tests simultaneously, using the same parameters. The samples were each heated up to 1000°C at a rate of 20°C per min while using 50mL of Nitrogen gas per minute to isolate the environment. The results of which would then be plotted as a graph of both weight% vs temperature and the first derivative of the weight% rate of change over time.

### 3.2 Mechanical Testing

To test the mechanical properties of the coupons we printed, we used the MTS Exceed electromechanical testing machine, and adhered to ASTM D638 to conduct our experiment properly. We took multiple measurements of the length and width of the cross-sectional area of each specimen, measured the gage length for each specimen, and recorded the crosshead displacement in millimeters and ramped loading in kilo Newtons with respect to time. We conducted 3 runs for 4 different specimens of each treatment group with various concentrations of fillers (+--, ++-, +-+, and +++). After completing these runs, we calculated the stress and strain of each run, and graphed them as shown in Figures 4-6. It is important to note that because the strain was estimated as a quotient of the crosshead displacement over the gage length. This is not representative of the actual strain experienced at the point of failure in the test coupon but is used as an accurate estimation of strain for analysis purposes.

### 3.3 Hirox Digital Microscope Imaging

The treatment group samples (+--, ++-, +-+, and +++) were then checked for pore occurrence and pore size ($\mu m^2$) by utilizing 3D Imaging techniques with low Range High Resolution Zoom Lens (MXB-2016Z) having the non-contact adapter (AD- 2016H) and Hirox RH-2000 software. For measuring pore occurrence and pore size of the samples, 120X magnification of the Zoom Lens was used.

### 3.4 Scanning Electron Microscope (SEM)

A scanning electron microscope (SEM) is an instrument for imaging topography and for obtaining material information of conductive specimens using a focused beam of high-energy electrons. The samples were coated with gold (Au) by using an Imaging Sputter Coater and with colloidal graphite for earthing the samples before inserting the samples for morphological analysis. The samples were then analyzed with a magnification of 80x, 200x, 1000x, and 2,000x. The SEM provided a detailed orientation of the dispersion and sizes of MCF and GMB throughout the sample. Energy Dispersive X-ray Spectroscopy (EDAX) was utilized to determine the molecular makeup of the sample. The EDAX showed if the MCF and GMB are dispersed evenly throughout the sample or if it was clumped in singular locations. [8]

## 4. RESULTS AND DISCUSSION

### 4.1 TGA and DTGA

Each of the samples had similar shaped results from the TGA analysis and resulted in a remaining char yield ranging from ~81% to 86%. In Figure. 3. below, the different ranges in which weight is lost are outlined from the TGA by the blue lines. The first and second phases are where excess moisture, solvents and monomers are evaporated. The third phase is where the main portion

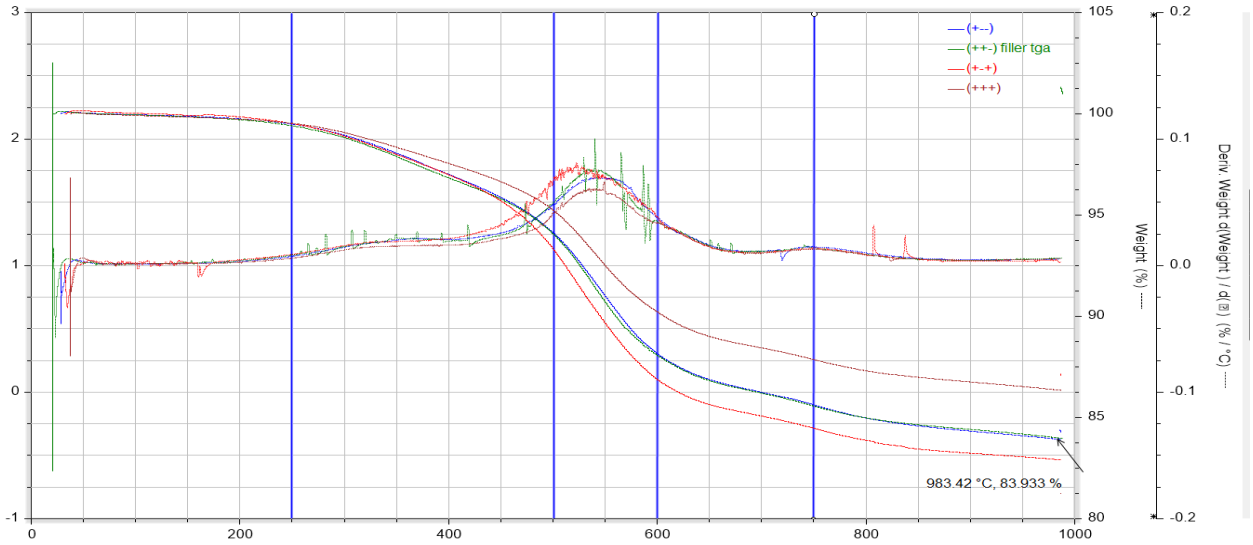


Figure 3. DTGA of the four tested treatment groups. The weight loss graph shows the different ranges in which weight is lost and first derivative graph shows where the most weight loss occurs.

of decomposition occurs and where a majority weight percent is lost. The fourth and final phase is the burning step of carbon, i.e., the carbon MCF and GMB. What is left afterwards is primarily ash residue and any remaining fillers that did not completely burn. In between phases four and five, the atmosphere within the TGA switches from pure nitrogen to regular air. This is to see what type of degradation would happen with oxidation added into the equation. In a pure Nitrogen environment, the TGA can monitor weight degradation entirely due to heat alone without the influence of oxidation.

When comparing the four treatment groups char yields to the filler ratio combination, one can see that without a high concentration of GMB, the presence of MCF does not affect the overall char yield. However, if GMB is present in a high concentration with a low concentration of MCF, the char yield lowers. When all three fillers are used in high concentration, the resulting char yield is the highest of all samples tested. This is due to the excellent thermal characteristics offered by the GMB and MCF. In Table 2, shown below, there is a detailed breakdown of each of the treatment groups. In the table, the maximum rate of decomposition for each sample was recorded to show how different compositions would affect the overall char yields and decomposition rates.

Table 2. Detailed analysis of DSC/TGA graphs

| Treatment Group | Heat Flow Highest Peak (W/g) | Highest Peak Temp (°C) | Heat Flow Lowest Peak (W/g) | Lowest Peak Temp (°C) | Char Yield (%) | Heat Flow Reversal Point (°C) |
|---|---|---|---|---|---|---|
| 1(+--) | 5.272 | 607.1 | 0.925 | 142.1 | 83.92 | 262 |
| 2(++-) | 7.982 | 684.6 | 1.873 | 196.3 | 83.93 | 337 |
| 3(+-+) | 7.156 | 633.7 | 1.966 | 172.9 | 82.93 | 309.6 |
| 4(+++) | 6.567 | 597.1 | 1.066 | 140.1 | 86.37 | 247.6 |

### 4.2 Mechanical Testing

As shown from Figure 4, we determined that the Ultimate tensile strength of these samples was lowest using the ++- concentration of fillers, and highest using the +++ concentration of fillers. From this we can determine that the Milled Carbon Fibers (MCF) and Graphitized micro balloons (GMB) increased composite strength with increasing concentration. These samples appear very linear, due to the large coefficients of determination ($R^2$ values). These samples all remain in the brittle failure region, with small percent elongation. However, the two treatment groups that contained higher concentrations of GMB elongated more than the treatment groups with low GMB concentrations. Using statistical analysis, the concentration of MCF and GMB was found to significantly impact composite ultimate tensile stress and elongation.

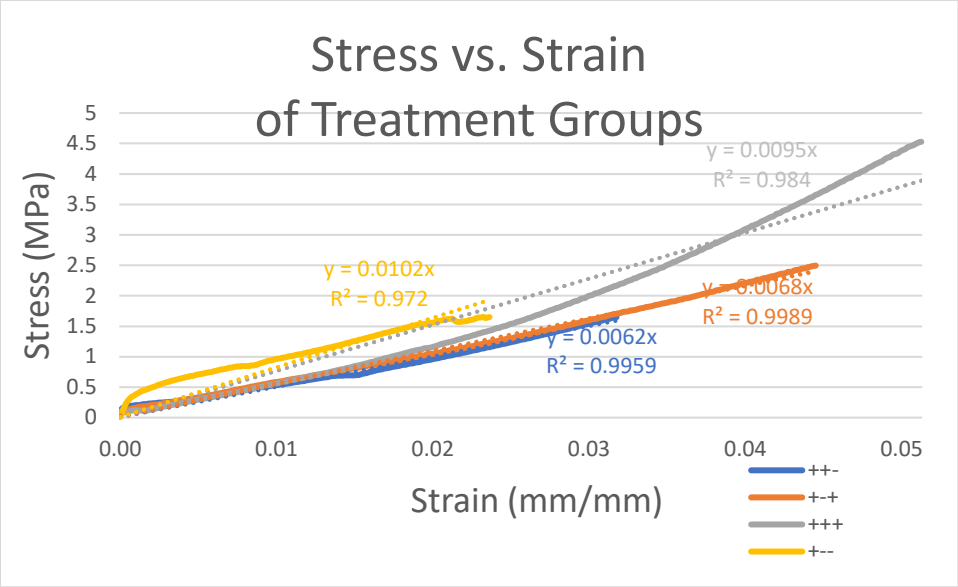


Figure 4. Stress vs. Strain of treatment

### 4.2.1 Statistical Analysis of Material Proprieties

The graphs did not properly illustrate young's modulus, Yield strength, or any necking. The main rise of the graph can be considered strain-hardening. Since these samples were able to be stretched to cause large strains, it resulted an undefined plastic range and did not follow Hooke's stress vs. strain law in the elastic region. Ultimate Tensile Strength was determined to be the value right before fracture, and the data was tested with an ANOVA test. The difference in elongation, or measurement that captures the amount a material will plastically and elastically deform up to fracture, was also determine through an ANOVA test. ANOVA is a statistical approach that divides observed variance data into various components for further testing. For three or more groups of data, ANOVA can be used to learn about the association between the dependent and independent variables. According to the test there is significant data to conclude that the Ultimate tensile strength and elongation changed with the addition of GMB and MCF. According to the data +++ resulted in the highest tensile strength and elongation followed by +-+, ++-, and finally +--. Table 3. below shows the mean, standard deviation, and std. Error of ultimate tensile strength for ++-, +-+, and +++. Table 4. Shows that the significant value in the difference of ultimate tensile strength is .002 which is less than .05, resulting in the conclusion that there is significant evidence to prove there is difference between the materials' tensile strength. Table 5. below shows the mean, standard deviation, and std. Error of elongation for ++-, +-+, and +++. Table 6. Shows that the significant value of the difference in elongation is .000 which is less than .05, resulting in the conclusion that there is significant evidence to prove there is difference between the materials' elongation.

Table 3. Ultimate tensile strength of (++-), (+-+), (+++),(+--) groups

| Value | N | Mean | Std. Deviation | Std. Error | 95% Confidence Interval for Mean | | Minimum | Maximum |
|---|---|---|---|---|---|---|---|---|
| | | | | | Lower Bound | Upper Bound | | |
| ++- | 3 | 1.5233 | 0.34530 | 0.19936 | 0.6656 | 2.3811 | 1.17 | 1.86 |
| +-+ | 3 | 2.4867 | 0.20502 | 0.11837 | 1.9774 | 2.9960 | 2.28 | 2.69 |
| +++ | 3 | 3.5100 | 0.87881 | 0.50738 | 1.3269 | 5.6931 | 2.92 | 4.52 |
| +-- | 3 | 1.4333 | 0.10504 | 0.06064 | 1.1724 | 1.6943 | 1.33 | 1.54 |
| Total | 12 | 2.2383 | 0.97250 | 0.28074 | 1.6204 | 2.8562 | 1.17 | 4.52 |

Table 4. ANOVA test results for Ultimate tensile strength

| ANOVA | | | | | |
|---|---|---|---|---|---|
| Value | Sum of the Squares | df | Mean Square | F | Sig. |
| Between groups | 8.514 | 3 | 2.838 | 12.018 | 0.002 |
| Within Groups | 1.889 | 8 | 0.236 | | |
| Total | 10.403 | 11 | | | |

Table 5. Elongation of (++-), (+-+), (+++), (+--) samples

| Descriptives | | | | | | | | |
|---|---|---|---|---|---|---|---|---|
| Value | N | Mean | Std. Deviation | Std. Error | 95% Confidence Interval for Mean | | Minimum | Maximum |
| | | | | | Lower Bound | Upper Bound | | |
| ++- | 3 | 0.0340 | 0.00173 | 0.00100 | 0.0297 | 0.0383 | 0.03 | 0.04 |
| +-+ | 3 | 0.0463 | 0.00231 | 0.00133 | 0.0406 | 0.0521 | 0.05 | 0.05 |
| +++ | 3 | 0.0523 | 0.00058 | 0.00033 | 0.0509 | 0.0538 | 0.05 | 0.05 |
| +-- | 3 | 0.0267 | 0.00306 | 0.00176 | 0.0191 | 0.0343 | 0.02 | 0.03 |
| Total | 12 | 0.0398 | 0.01068 | 0.00308 | 0.0331 | 0.0466 | 0.02 | 0.05 |

Table 6. ANOVA test results for Elongation

| ANOVA | | | | | |
|---|---|---|---|---|---|
| Value | Sum of the Squares | df | Mean Square | F | Sig. |
| Between groups | 0.001 | 3 | 0.000 | 90.198 | 0.000 |
| Within Groups | 0.000 | 8 | 0.000 | | |
| Total | 0.001 | 11 | | | |

### 4.3 Hirox Digital Microscope Imaging

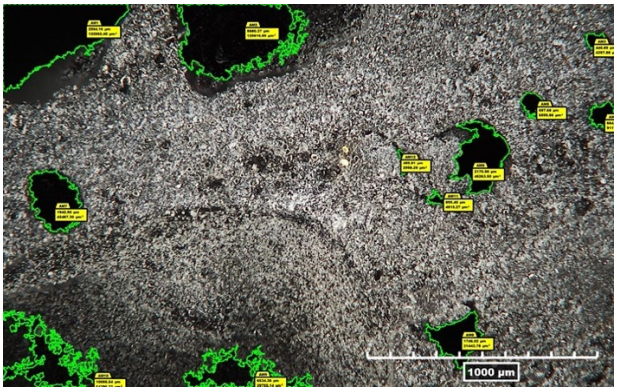


Figure 5. Hirox Digital Microscope image of (+--) group

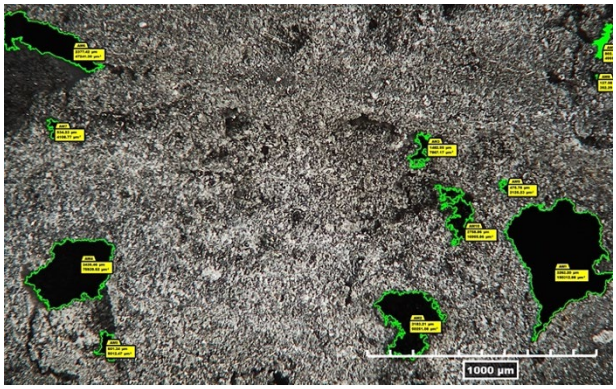


Figure 6. Hirox Digital Microscope image of (++-) group

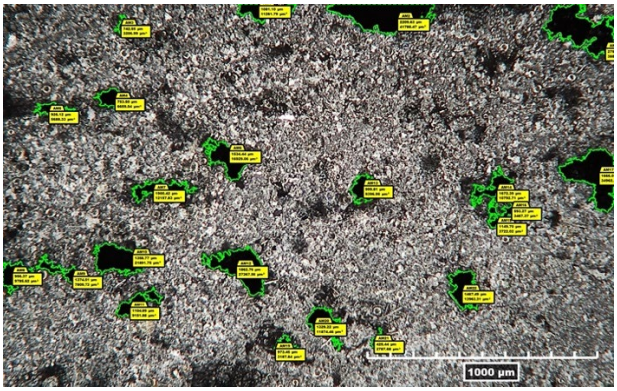


Figure 7. Hirox Digital Microscope images of (+-+) group

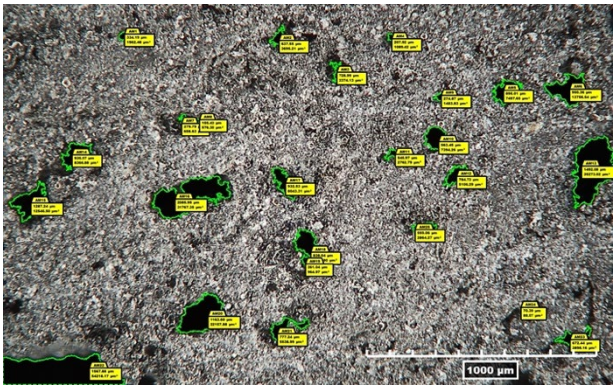


Figure 8. Hirox Digital Microscope images of (+++) group

Table 7. Pore measurement of treatment group samples (+--, ++-, +-+, and +++)

| Parameter | +-- | ++- | +-+ | +++ |
|---|---|---|---|---|
| Average Pore Size ($\mu m^2$) | 41137.50 | 33192.87 | 13941.99 | 9694.48 |
| % Pore Coverage ($\mu m^2$) | 11.21% | 6.97% | 8.29% | 5.50% |
| Total Pore Occurrence | 12 | 11 | 22 | 25 |
| Range of Pore Size ($\mu m^2$) | 126818.60 | 149960.60 | 39000.79 | 54130.10 |

From Table 7, it is evident that the average pore size is higher in +-- group, which means the highest pore coverage of 11.21% in this group. However, the most pore occurrences are found in +++ group whereas the range of pore size is higher in ++- group.

### 4.4 Scanning Electron Microscope Imaging

The morphological analysis of milled carbon fiber (MCF) was investigated with the help of FEI-SEM. In Figure 9, the SEM micrographs show that there is minimal damage to the GMB following processing and curing. There does not appear to be major agglomerations occurring, supporting that the mechanical mixing was sufficient to ensure particle dispersion.

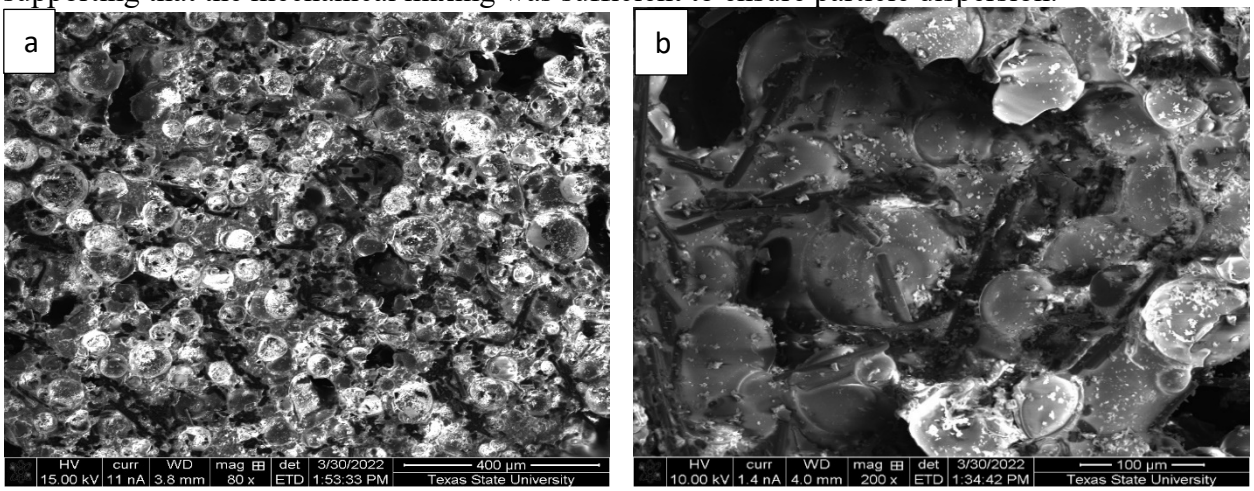


Figure 9. SEM Micrographs
a. Induction cured Milled Carbon Fiber (MCF) (80x)
b. Damaged micro balloons (200x)

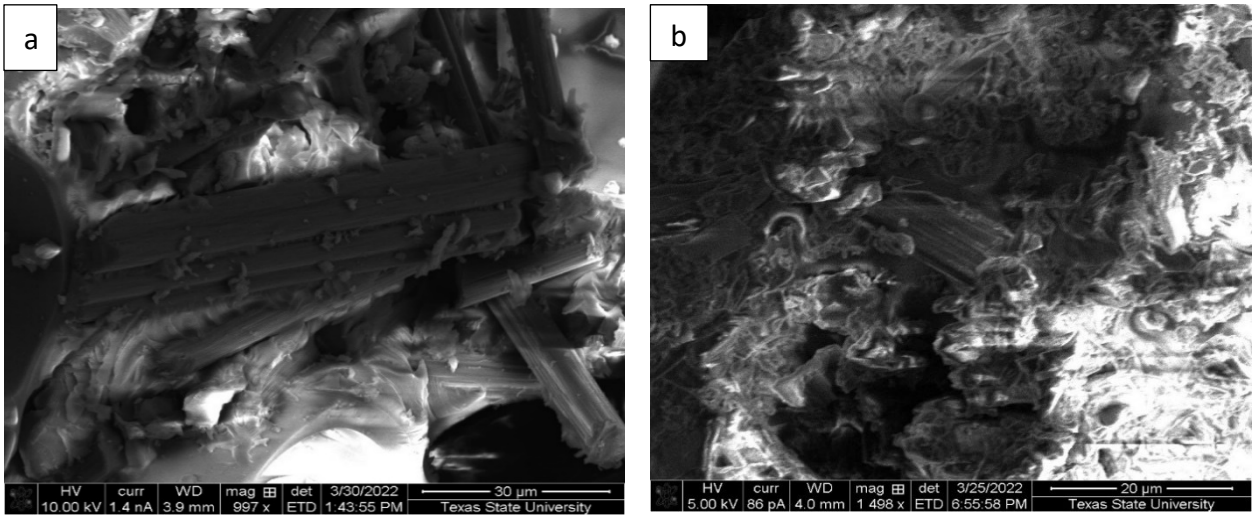


Figure. 10. SEM Micrograph of MCF Agglomeration of:
a. Induction cured sample
b. Oven cured sample

Figure 10a and 10b show MCF agglomeration in induction curing as compared to the MCF agglomeration in over curing. This indicates that due to the presence of Fe3O4 which enables the induction curing and ensures the high agglomeration and high dispersion of MCF, GMB. Hence,

increases the mechanical properties i.e. lowers the porosity and pore size compared to the oven cured samples. We investigated the aspect ratio of microfiber both in induction cured sample and oven cured sample. Figure 11a and 11b show that there is no significant difference in terms of aspect ratio during induction curing and oven curing. This indicates that carbon fiber did not get damaged due to induction curing resulting in the same material properties as of oven cured sample.

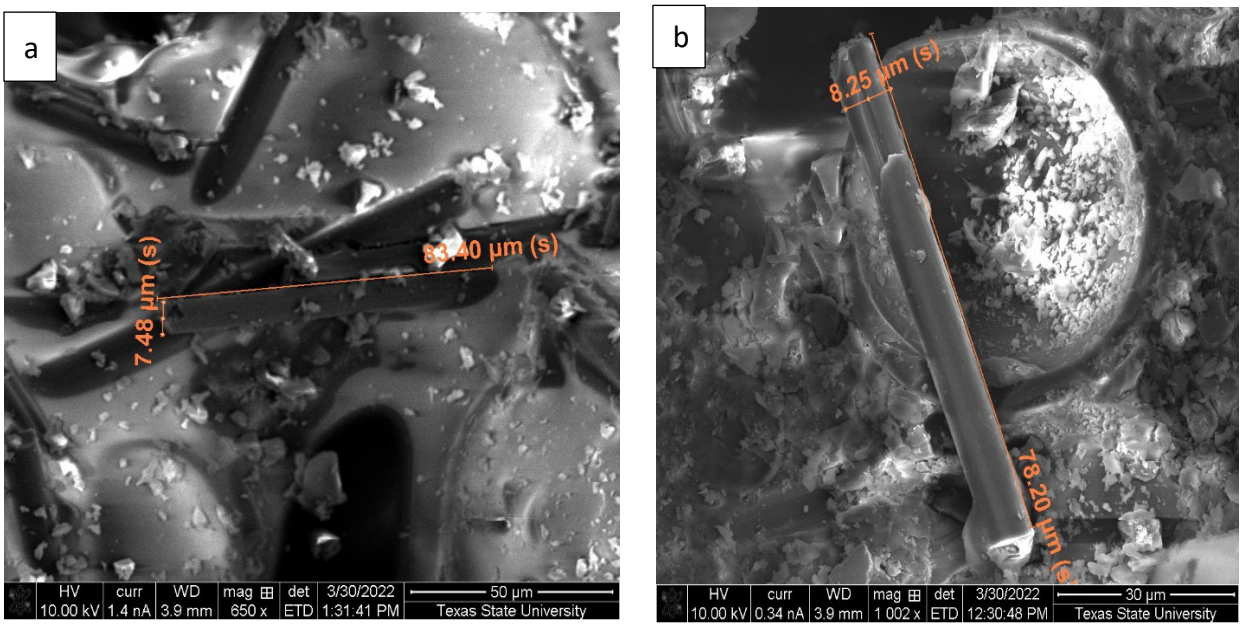


Figure 11. SEM Micrograph showing
Aspect Ratio of Milled Carbon Fiber of:
a. Induction cured sample
b. Oven cured sample

Similarly, we analyzed both induction cured and oven cured samples in energy-dispersive X-ray spectroscopy (EDAX) to characterize the constituent's aggregation in the samples. Figures 12 and 13 show the live mapping of induction cured sample and oven cured sample. The mapping analysis shows that the MCF is evenly dispersed.

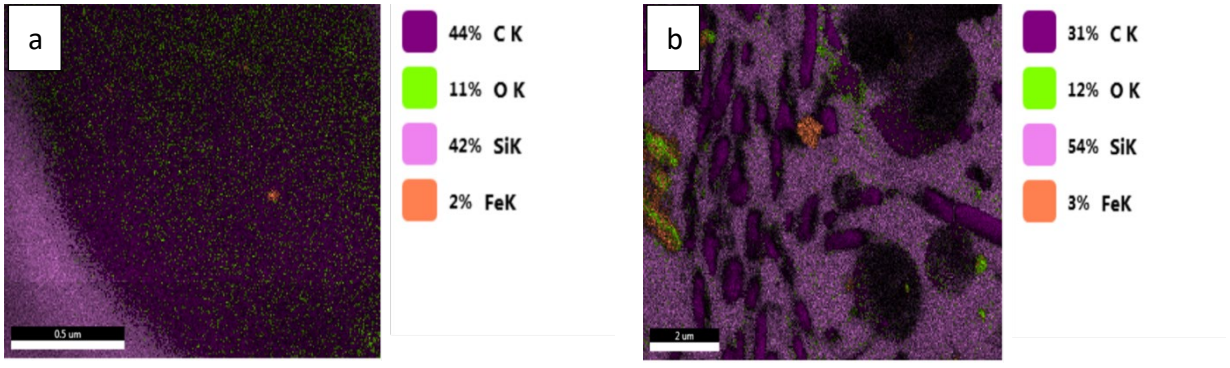


Figure 12. Live mapping using EDAX Map Analysis of:
a. Induction cured sample
b. Oven cured sample

The EDAX map analysis in Figure 13, shows that during induction curing the iron particles are evenly dispersed across and there is no significant agglomeration of iron. This indicates that mechanical mixing was sufficient for the dispersion of the iron particles across the resin matrix. Hence, these evenly dispersed iron particles helped to optimize the utilization of hysteresis heat during the induction curing process.

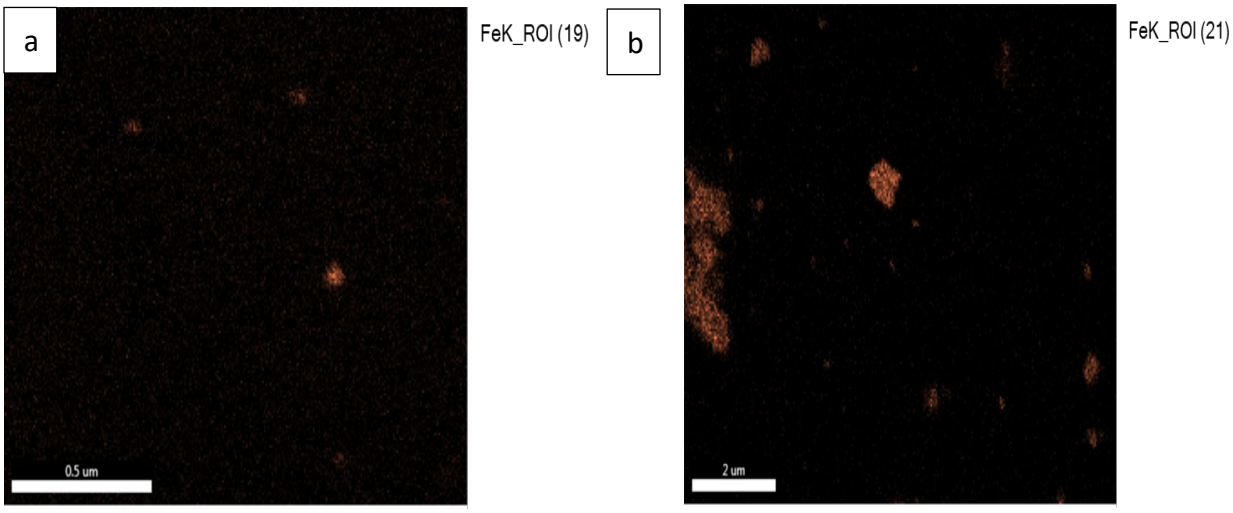


Figure 13. EDAX map imaging of Iron Particle dispersion of:
a. Induction Cured sample
b. Oven Cured sample

## 5. CONCLUSION

The growing use of lightweight composite materials in additive manufacturing has paved the way for our research to study the impact of induction curing on additively manufactured thermoset composites. Considering the limitation of printing thermoset composite parts, this research has determined a precise ratio of reinforcement fillers to magnetic susceptor for optimizing curing time and maximizing the mechanical properties. The primary focus was associated with testing different loading levels of composites fillers using susceptor curing. For exploring such high temperature material that incorporates additive manufacturing and induction heating, multiple reinforcing fillers were required. These reinforcing fillers were evenly dispersed to promote the release of exothermic heat and aid in the curing of the surrounding thermoset material while printing. Due to its ferrimagnetic characteristics, $Fe_3O_4$ was utilized as a susceptor in the filler material to initiate induction curing. Milled carbon fiber material was added to the composite to improve overall mechanical characteristics and graphitized micro balloons were added to improve the strength-to-weight ratio. Finally, the performance measurements of the resulting induction cured composite samples were evaluated and demonstrated in comparison with the oven-cured composite samples. Thermogravimetric analysis was performed and showed that the highest remaining char yield was allowed due to high concentrations of each filler material, and most of the weight percent loss occurred 450°C to 600°C. The SEM micrograph showed that the MCFs were dispersed evenly in the resin matrix without damaging the fibers. EDAX live mapping indicated that the iron particles were evenly dispersed resulting in better induction capacity of the samples for the induction curing.

## 6. ACKNOWLEDGEMENTS

The authors would like to thank every member of Analysis Research Service Center (ARSC) and Advanced Composites Laboratory of Texas State University for their support during the experiments of this research. We would also like to appreciate the help of Dr. Jitendra S. Tate for providing continuous guidelines towards our research objective.

## 7. REFERENCES

1. Nawafleh, N. and E. Celik, *Additive manufacturing of short fiber reinforced thermoset composites with unprecedented mechanical performance.* Additive Manufacturing, 2020. **33**: p. 101109.

2. Blok, L.G., et al., An investigation into 3D printing of fibre reinforced thermoplastic composites. Additive Manufacturing, 2018. 22: p. 176-186.

3. Compton, B.G. and J.A. Lewis, 3D-printing of lightweight cellular composites. Advanced materials, 2014. 26(34): p. 5930-5935.

4. Yungwirth, Christian J. "Induction Curing of a Phase-Toughened Adhesive". Aberdeen Proving Ground, Md. : Army Research Laboratory, 2003.

5. Cheng, X. & Zhou, Y. & Charles, A. & Yu, Y. & Islam, M. & Peng, S. & Wang, J. & Rider, A. & Lim, M. & Timchenko, V. & Wang, C. 2021. Materials & Design, Vol. 210. Sydney, Australia. Elsevier. https://doiorg.libproxy.txstate.edu/10.1016/j.matdes.2021.110076.

6. Bayerl, T., Schledjewski, R., & Mitschang, P. (2012). Induction Heating of Thermoplastic Materials by Particulate Heating Promoters. Polymers and Polymer Composites, 333–342. https://doi.org/10.1177/096739111202000401

7. Bayerl, T. & Duhovic, M. & Mitschang, P. & Bhattacharyya, D. 2013. Composites Part A: Applied Science and Manufacturing, Vol. 57. Kaiserslautern, Germany. Elsevier. https://doi.org/10.1016/j.compositesa.2013.10.024.

8. Schmitt R. (2014) Scanning Electron Microscope. In: The International Academy for Production Engineering, Laperrière L., Reinhart G. (eds) CIRP Encyclopedia of Production Engineering. Springer, Berlin, Heidelberg. https://doi.org/10.1007/978-3-642-20617-7_6595.